ACS APPLIED MATERIALS & INTERFACES

Research Article

www.acsami.org

Protein-Mediated Layer-by-Layer Synthesis of TiO_2(B)/Anatase/Carbon Coating on Nickel Foam as Negative Electrode Material for Lithium-Ion Battery

Xiaobo Wang, Yong Yan,† Bo Hao, and Ge Chen*

College of Environmental & Energy Engineering, Beijing University of Technology, Pingleyuan 100, 100124, Beijing, People's Republic of China

Supporting Information

ABSTRACT: Through an aqueous, protein-mediated layer-by-layer titania deposition process, we have fabricated a protamine/titania composite layer on nickel foam. The coating was composed of amorphous carbon and TiO_2(B)/anatase nanoparticles and formed upon organic pyrolysis under a reducing atmosphere (5% H_2−Ar mixture). X-ray diffraction analyses, Auger electron spectroscopy, and high-resolution transmission electron microscopy revealed that the obtained coatings contained fine monoclinic TiO_2(B) and anatase nanocrystals, along with amorphous carbon. Moreover, the coating can be used as a binder-free negative electrode material for lithium-ion batteries and exhibits high reversible capacity and fast charge−discharge properties; a reversible capacity of 245 mAh g^{-1} was obtained at a current density of 50 mA g^{-1}, and capacities of 167 and 143 mAh g^{-1} were obtained at current densities of 1 and 2 A g^{-1}, respectively.

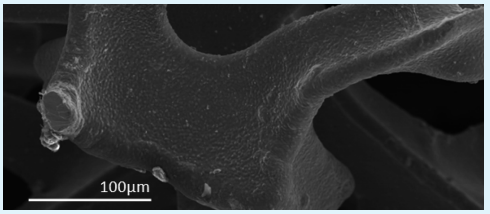

KEYWORDS: *TiO_2(B), mineralization, protamine, layer-by-layer, nickel foam, lithium ion batteries*

INTRODUCTION

Nature possesses the ability to produce biominerals with exquisite nanostructures under inherently mild conditions of low temperature, ambient pressure, and near-neutral pH.[1] Mimicking biomineralization has great potential to control inorganic structures and is fast becoming an important next-generation inorganic synthesis method.[2] Recent insight into the molecular mechanisms of biomineralization has enabled biomimetic approaches for the synthesis of non-natural but technologically interesting materials under mild reaction conditions.[3−5] In particular, biomineralization of TiO_2 has attracted much attention, because of its many promising applications in environmental and energy areas.[6] Besides the mild synthesis conditions, the bioinspired approach might provide a new pathway to tailor the morphology, polymorphism, and elemental doping of titania with significant advantages over traditional methods.[7] For example, the anatase phase usually forms first in all solution titania synthesis pathways, and the phase transformation from anatase to rutile usually occurs during a hydrothermal process under extremely acidic conditions;[8−10] however, a highly crystalline rutile phase can be obtained at room temperature and neutral pH when using recombinant silaffins as biomineralization agents.[11] It is well-known that the physicochemical properties of titania strongly influence its application performance; thus, it is of interest to synthesize titania with tailored properties through biomineralization pathways in the context of green chemistry, and for potential application in many technological devices.

Because of the advantages of low cost, low environmental impact, safety, and rate capability, the various polymorphs of TiO_2 (anatase, rutile, and TiO_2(B)) have been widely studied and TiO_2 is considered to be a good alternative to the carbon-based anode materials in lithium-ion batteries.[12] Compared with the anatase and rutile phases, the TiO_2(B) exhibits more open channels in its lattice as well as characteristic pseudo-capacitive behavior, resulting in easier Li-ion access to the crystal structure and faster charge−discharge capability.[13] However, the majority of approaches to prepare nanostructured TiO_2(B) involve the use of layered titanate, which is often prepared from titania powder by alkaline hydrothermal treatment (~100−150 °C, 8−10 M NaOH or KOH).[14−22] Recently reported hydrothermal or solvothermal treatments avoid the use of a high concentration of alkali.[23−26] Nevertheless, corrosive titanium precursors ($TiCl_3$ or $TiCl_4$) and chemicals ($NH_3{\cdot}H_2O$, H_2O_2, H_2SO_4) are required, which is undesirable, from an environmental perspective. Therefore, it is highly desirable but challenging to synthesize nanostructured TiO_2(B) as an electrode material through a facile and "green" synthesis route.

In this paper, we demonstrate the use of an aqueous, protein-enabled layer-by-layer (LbL) titania deposition process to fabricate protein−titania composite coatings on nickel foams. The coatings are composed of amorphous carbon and TiO_2(B)/anatase nanoparticles, and are obtained upon organic pyrolysis at 500 °C under a reducing atmosphere (5% H_2−Ar mixture). The method is based on a recently developed LbL

Received: January 8, 2013
Accepted: April 2, 2013
Published: April 18, 2013

   dx.doi.org/10.1021/am4000744 | ACS Appl. Mater. Interfaces 2013, 5, 3631−3637

mineralization process that employs protamine, which is a relatively inexpensive and readily-available arginine-rich protein harvested from a variety of fish, as a biomimetic mineralization agent for inducing the formation of a TiO_2 coating from a titanium(IV) bis(ammonium lactato) dihydroxide (Ti-BALDH)-bearing solution.[27] Prior work has involved deposition on diatom frustules,[28] alumina templates,[29] silica spheres,[30] and poly(sodium-*p*-styrenesulfonate) (PSS)-doped $CaCO_3$ spheres,[31] and subsequent organic pyrolysis in air resulting in the crystalline anatase titania coating.[28,29,31]

Nickel foam is used here as an ideal electrode substrate, because of its high electronic conductivity, low weight, and three-dimensional (3D) cross-linked grid structure, providing high porosity and surface area. However, unlike the negatively charged surface of diatom frustules, silica spheres, alumina, and PSS-doped $CaCO_3$ particles, the surface of nickel foam is often inert and hydrophobic, making it difficult to adsorb cationic protamine. To overcome this problem, the nickel foam in our experiment was modified with a hydrophilic polydopamine (PDA) layer via the self-polymerization of dopamine simply by dipping it into a dopamine solution at room temperature. As a mimic of the specialized adhesive foot protein, PDA is known to attach to almost all wet substrates,[32] and the PDA layer has a net negative charge at pH >7.[33] Considering the higher isoelectric point of protamine (>12), it is reasonable to assume that the protamine successfully adsorbs to the PDA layer by electrostatic interaction in a high pH environment (pH 8.5). The PDA-coated nickel foams were subsequently exposed in a repetitive alternating fashion to protamine and then to an aqueous Ti-BALDH solution to build up the titania-containing coating.

Interestingly, we observed, for the first time, the formation of TiO_2(B) nanoparticles when the organic pyrolysis was performed under a reducing atmosphere (5% H_2–Ar mixture). Such a bio-inspired approach to forming TiO_2(B) nanomaterials has many merits. First, except for organic pyrolysis, the entire synthetic procedure is carried out at room temperature and at neutral (or near neutral) pH in an aqueous system, and no corrosive titanium precursors or chemicals are needed. Second, the thickness of the coating can be easily tuned by adjusting the number of LbL cycles. Finally, as a potential electrode material, the carbon derived from the pyrolysis of protamine can form a continuous 3D conductive network among coatings, thereby improving its performance in lithium-ion batteries.[34] More interestingly, the obtained TiO_2(B)/anatase/carbon-coated nickel foam can be used as a binder-free electrode in lithium-ion batteries and exhibits high reversible capacity and fast charge–discharge properties. A high reversible capacity of 240 mAh g^{-1} was obtained at a current density of 50 mA g^{-1}, and the capacities of 163 and 147 mAh g^{-1} were obtained at current densities of 1 A g^{-1} and 2 A g^{-1}, respectively.

EXPERIMENTAL SECTION

Preparation of TiO_2(B)/Anatase/Carbon Coating on Nickel Foam. Protamine (Sigma–Aldrich), Ti-BALDH solution (50% Alfa Aesar), dopamine (Sigma–Aldrich), and nickel foam (Changsha Liyuan Newmaterial Co.) were purchased commercially. A polydopamine (PDA) layer was fabricated on the nickel foam by soaking the nickel foam in an alkaline dopamine solution (pH 8.5, 0.5 M) at room temperature for 12 h. The PDA-functionalized nickel foams were then exposed in alternating fashion to buffered aqueous solutions of protamine (1 mg/mL) and the titania precursor solution, Ti-BALDH (5 wt %) for one half hour, respectively. The pH of the first protamine solutions was higher (pH 8.5) than that of the subsequent solutions (pH 7.0) to ensure the successful adsorption of protamine on the PDA layer. After ~20–40 LbL cycles, the nickel-foam-coated protamine/titania composite was annealed in a reducing atmosphere (5% H_2–Ar) at 500 °C for 3 h. Finally, a coating composed of carbon and TiO_2(B)/anatase was formed on the nickel foam.

Material Characterization. X-ray diffraction (XRD) was carried out on a Bruker D8 Advance diffractometer using the Cu Kα lines (40 kV, 40 mA), and data were acquired from in 2θ range of 10°–80° at a rate of 0.02° s^{-1}. Transmission electron microscopy (TEM) images were taken using a Tecnai F20 microscope on powder samples deposited onto a copper microgrid coated with carbon at an accelerating voltage of 200 kV. Thermogravimetric analysis (TGA) was conducted on a Seiko Instruments 6300 TG-DTA device with the sample heated from 20–800 °C in air at a rate of 5 °C min^{-1}. For XRD, TEM, and TGA characterization, samples were pretreated with 3 M HCl at 80 H for 3 h to remove the substrate (nickel foam), and the obtained powder was washed with distilled water several times and dried in a vacuum oven overnight at 100 °C. The prepared powder was then used for XRD, TEM, and TGA characterization. For high-resolution transmission electron microscopy (HRTEM) characterization of the TiO_2(B)/anatase/carbon coating, the obtained powder was further embedded in resin, followed by ion milling. Zeta potential measurements were conducted on an Anton Paar SurPASS instrument. Scanning electron microscopy (SEM) images were obtained from a Hitachi Model S-4300 instrument operated in high vacuum mode. A PHI-700 (ULVAC-PHI) instrument was used for Auger electron spectroscopy (AES) analysis. An Axis Ultra (Kratos Analytical, Ltd.) instrument with monochromatized Al Kα radiation and an energy resolution of 0.48 eV was used for X-ray photoelectron spectroscopy (XPS), and the shift of the binding energy was corrected using the C 1s level at 284.8 eV.

Electrochemical Measurement. The obtained TiO_2(B)/anatase/carbon-coated nickel foams were vacuum dried overnight at 100 °C and cut off as binder-free electrodes with a TiO_2 loading of ~1.5–2.0 mg. The model cell was the 2032 coin cell. The amount of active material (TiO_2) on the foam was characterized by inductively coupled plasma–atomic emission spectrometry (ICP-AES) (IRIS Intrepid ER/S), pretreatments includes the removal of carbon by calcination, and the subsequent dissolution of metal and oxides by a mixture of aqua regia and hydrofluoric acid solution. Glass fiber (GF/D) from Whatman was used as a separator. Pure lithium foil (Aldrich) was used as the counter electrode, and the electrolyte used was 1 M $LiPF_6$ in a 50:50 w/w mixture of ethylene carbonate and diethyl carbonate. Cell assembly was conducted in a re-circulating argon glove box, where both the moisture and oxygen contents were <0.1 ppm. Galvostatic electrochemical experiments were carried out with a Neware battery tester (Shenzhen, China), and the discharge–charge experiments were tested at different current densities in a voltage range of 1.0–3.0 V. Cyclic voltammetry (CV) measurements of the electrodes were performed on an electrochemical workstation (VMP3).

RESULTS AND DISCUSSION

The presence of a PDA layer can be deduced from the presence of the N and C species, determined by XPS (Figure 1). The N/C molar ratio for the PDA layer is 0.115, which is close to the theoretical value of pure dopamine (0.125) and the same as pH-induced PDA layers reported for other substrates.[35] Nevertheless, a trace amount of nickel was observed in the full spectrum, indicating either that the thickness of the PDA layer was very small or that the coverage was not uniform. A high-resolution XPS analysis of the nickel species is provided in Figure S1 in the Supporting Information; the binding energy was determined to be 855.7 eV, corresponding to $Ni(OH)_2$, which might be attributed to a thin nickel oxide layer on the nickel foam. The PDA-coated nickel foams were then exposed in alternating fashion to buffered aqueous solutions of protamine and the titania precursor, Ti-BALDH, as illustrated

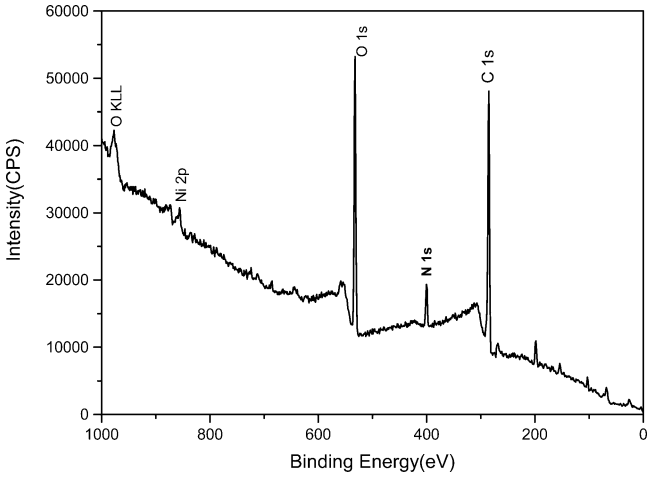

Figure 1. XPS analysis revealing the presence of C, O, N, and the trace amount of Ni on the surfaces of the polydopamine-coated nickel foam.

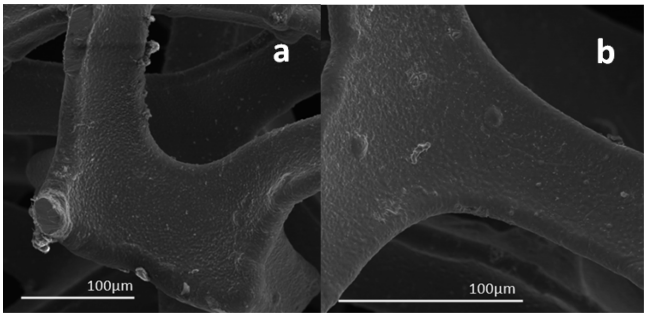

Figure 2. Scanning electron microscopy (SEM) image of protamine/Ti−O-coated nickel foam (exposure to 20 protamine/TiBALDH cycles) (a) before and (b) after organic pyrolysis. Bar = 100 μm.

in Scheme 1. The LbL mineralization process was monitored by zeta potential measurements taken at every step during the first 10 cycles of TiO deposition; an oscillation in the measured zeta potential was detected after each alternating exposure to the buffered protamine and Ti-BALDH solutions (see Figure S2 in the Supporting Information), which is consistent with the presence of an external layer of positively charged protamine molecules or of negatively charged Ti-BALDH/titania, respectively.

SEM images of a protamine/TiO-bearing composite coating on nickel foam after 20 protamine/TiBALDH deposition cycles are shown in Figure 2a. A continuous, conformal coating was observed on the foam. AES was further used to verify the elemental composition of the surface and inside of the coating layer. The existence of C, Ti, O, and small amount of Ni species on the surface of the coating layer is demonstrated in Figure 3a. After sputtering for 5.6 min (the sputter rate was 37 nm min^{-1} for thermal oxidation of the SiO_2/Si substrate), only Ni was observed in the spectrum (see Figure S3 in the Supporting Information). The atomic content of C, Ti, O, and Ni with sputtering time is given in Figure 3b; the content of C remains stable at 23% and the content of Ti remains stable at 17%, suggesting that the obtained protamine/TiO layer is uniform. Furthermore, we have observed that the content of Ti species begins to decrease after 2.6 min of sputtering, allowing us to deduce that the thickness of protamine/TiO layer is ∼96 nm (2.6 min × 37 nm min^{-1}). Although there is some uncertainty in the estimated coating thickness value of 96 nm due to the different etching rates for the 20 deposition cycles, the result agrees well with previously reported data.[29] The protamine/TiO-coated nickel foam was further characterized by XPS, which demonstrated the existence of Ti, O, N, and C species (see Figure S4 in the Supporting Information). The N 1s spectrum showed a band at 400.01 eV attributed to the amide group from protamine (Figure S4 in the Supporting Information), and the O 1s spectrum comprised three bands at 529.97, 531.38, and 532.60 eV, which can be assigned to TiO−Ti, O═C, and C−O bonds, respectively; the latter two species might also be from protamine[27,31] (see Figure S4 in the Supporting Information).

The coated foams were then heated at a rate of 5 °C min^{-1} from room temperature to 500 °C in a 5% H_2−Ar mixture, and held at this temperature for 3 h to allow for water removal, organic pyrolysis, and titania crystallization. The SEM image of

Scheme 1. Illustration of the Protein-Mediated Layer-by-Layer Deposition Assisted the Synthesis of a TiO_2(B)/Anatase/Carbon Coating on Nickel Foam

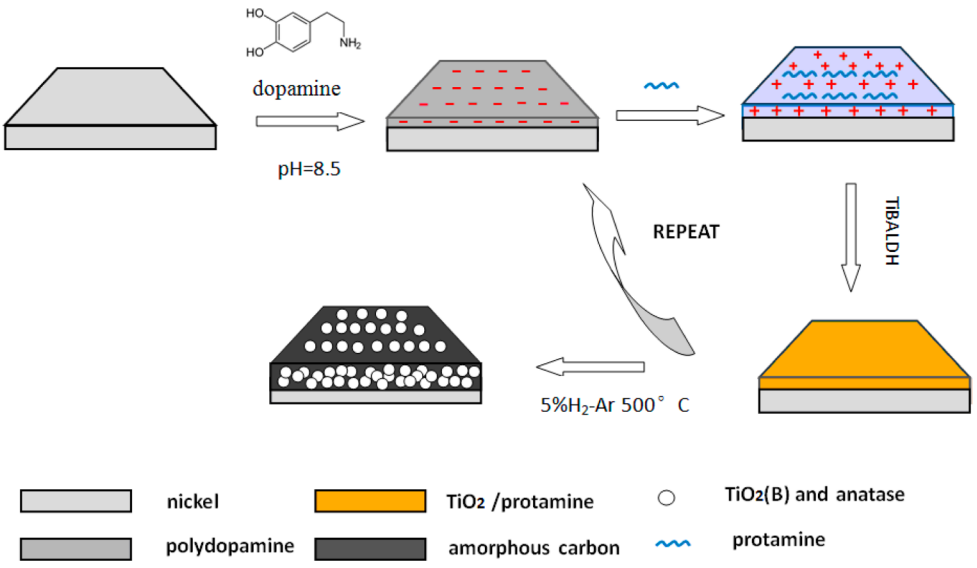

dx.doi.org/10.1021/am4000744 | ACS Appl. Mater. Interfaces 2013, 5, 3631−3637

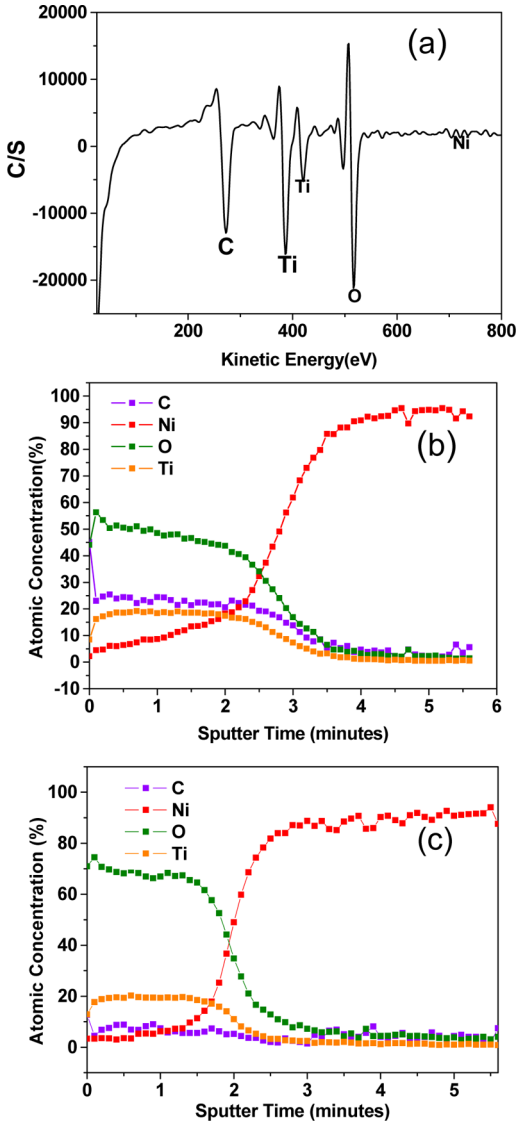

Figure 3. (a) Auger electron spectroscopy (AES) analysis indicated the presence of Ti, C, O and the trace amount of nickel on the surfaces of the protamine/titania composite layer coated on nickel foam. The change of atomic content of C, O, Ti and Ni with sputtered time for protamine/Ti−O-coated nickel foam (b) before and (c) after organic pyrolysis.

the annealed sample revealed a continuous, conformal layer on the nickel foam, similar to that of the as-prepared protamine/TiO layer (see Figure 2b). AES analysis revealed that the atomic content of carbon decreased from 23% to 8% after organic pyrolysis, while the content of titanium slightly increased from 17% to 20% (see Figure 3c). Figure S5a in the Supporting Information shows the C 1s spectra of the coating material before organic pyrolysis. The C 1s spectrum has four main peaks, corresponding to the following bonds: aliphatic C*H−CH (284.8 eV), which may have originated from adventitious carbon (the respective carbon species are marked by an asterisk), and the peaks at 285.8 eV, 286.6 eV and 288.3 eV might be attributed to −C*−NH_2, amidic N−C*H−C═O, and amidic N−CH−C*═O, respectively, which was believed to have come from protamine. Besides the aforementioned four peaks, a new peak was observed at 284.3 eV after pyrolysis (see Figure S5b in the Supporting Information), which was believed to have come from carbon; and the peak (at 285.8, 286.6, and 288.3 eV) areas decreased dramatically, indicating that most of the protamine was pyrolyzed to carbon. In addition, the binding energy of Ti $2p_{3/2}$ is 458.8 eV (Figure S6 in the Supporting Information), indicating the presence of Ti^{4+} species; there was no evidence of Ti^{3+} species in the XPS spectrum.

Thermogravimetric analysis (TGA) was used to define the exact amount of amorphous carbon in the materials (see Figure S7 in the Supporting Information). The minor weight loss (~3.9%) before 150 °C might be due to the removal of adsorbed water, and the major weight loss (~16.2%) between 150 °C and 650 °C might be due to the decomposition of carbon. The XRD pattern of the coating before and after organic pyrolysis is shown in Figure 4. Although the as-prepared protamine/titania composite has an amorphous structure, the diffraction peaks at 14.7°, 28.8°, and 44.0° can be clearly indexed to the (001), (002), and (003) planes of the monoclinic TiO_2(B) phase (corresponding to JCPDS File Card No. 74-1940) in the coating annealed in the 5% H_2−Ar mixture. Some minor peaks can be identified as the tetragonal anatase phase, and the major diffraction peak at 25.4° could be either TiO_2(B) (110) or the anatase (101) plane. Only the anatase phase was obtained in samples that were calcined in air and argon (see Figure S8 in the Supporting Information). The formation of the TiO_2(B) phase is interesting: it is reasonable to assume that the reducing atmosphere plays a pivotal role in the formation of the TiO_2(B) phase; however, a comprehensive investigation into this is outside of the scope of the present work.

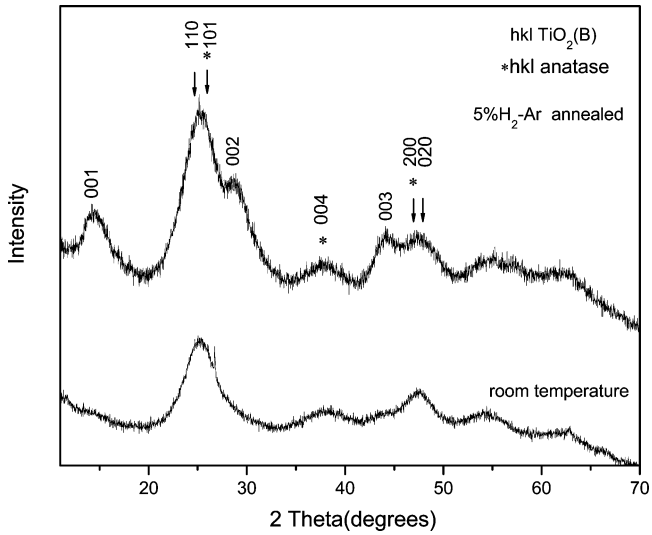

Figure 4. XRD pattern of as prepared protamine/titania composite coating on nickel foam before organic pyrolysis (bottom spectrum) and after organic pyrolysis (top spectrum).

In the TEM image of the calcined sample shown in Figure 5a, a large amount of nanoparticles are observed to be embedded in the amorphous matrix. Confirmation that the nanoparticles are TiO_2(B) phase is also obtained from the HRTEM image (Figures 5b and 5c); lattice spacings of 0.357 and 0.201 nm can be attributed to the (110) and (003) reflections from the TiO_2(B) structure, and the corresponding fast Fourier transform (FFT) in Figure S9 in the Supporting Information reveals lattice planes of (001), (110), (310), (003),

dx.doi.org/10.1021/am4000744 | ACS Appl. Mater. Interfaces 2013, 5, 3631−3637

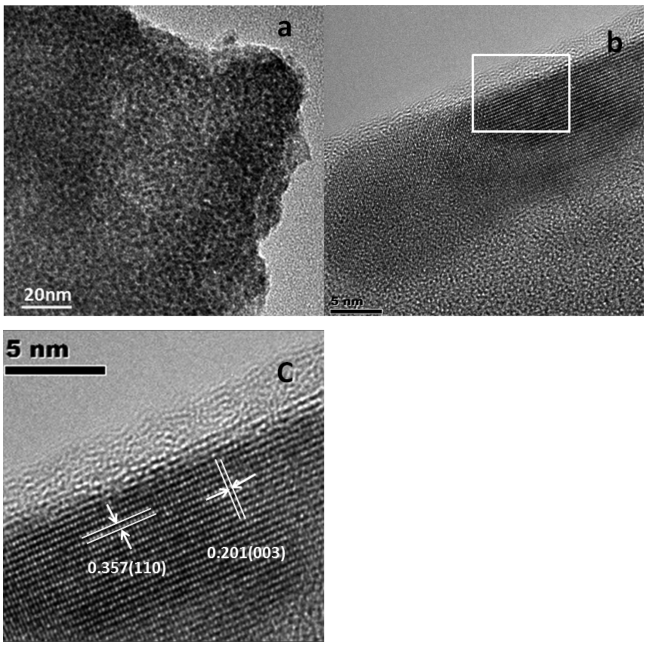

Figure 5. (a) Transmission electron microscopy (TEM) image of 5% H_2–Ar annealed coatings. (b) High-resolution transmission electron microscopy (HRTEM) image of 5% H_2–Ar annealed coatings. (c) Partial enlarged view of panel b (selected area); the lattice spacings of 0.357 nm and 0.201 nm were attributed to the (110) and (003) reflections from the TiO_2(B) structure.

and (020) that exactly correspond to the monoclinic structure of the TiO_2(B) phase. An amorphous layer was observed on the crystalline TiO_2(B) nanoparticles (Figure 5c), which could be either carbon or amorphous titania; such a layer was not found in the sample annealed in air (see Figure S10 in the Supporting Information).

The electrochemical performance of this material was evaluated in lithium half-cells. Cyclic voltammetry (CV) curves obtained at a scan rate of 0.1 mV s^{-1} are shown in Figure 6a. There are three pairs of peaks in the CV. The observation of a pair of peaks located between 1.9 and 1.7 V (denoted as peak A) is the typical response expected for solid-state diffusion of lithium intercalation in the anatase phase. The other two pairs of peaks located at ~1.6 V and ~1.5 V (denoted as peak S) reflect the characteristic pseudo-capacitive behavior of lithium storage in TiO_2(B);[36] theoretical studies have shown that this pseudo-capacitive behavior originates from the unique sites and energetics of lithium absorption and diffusion in the TiO_2(B) structure.[37−39] Note the peak current of peak A is much smaller than that of peak S at a slow scan rate (0.1 mV s^{-1}). This could be due to the small-sized anatase nanoparticles encapsulated in the carbon, resulting in a large decrease in lithium intercalation and increase in interfacial lithium storage.[40] It is also possible that the small peak A value reflects the small amount of anatase phase in the coating.[21] Because the pseudocapacitive current scales with the first power of scan rate and the diffusion current scales with the square root of the scan rate, we suppose that fast pseudocapacitive lithium transport dominates the lithium storage process at high currents, thus, resulting in the fast charge−discharge properties.

Galvanostatic discharge−charge measurements were carried out over a voltage range from 1.0 to 3.0 V to evaluate the electrochemical performance of the TiO_2(B)/anatase/carbon-coated nickel foam. In Figure 6b, potential−capacity profiles of

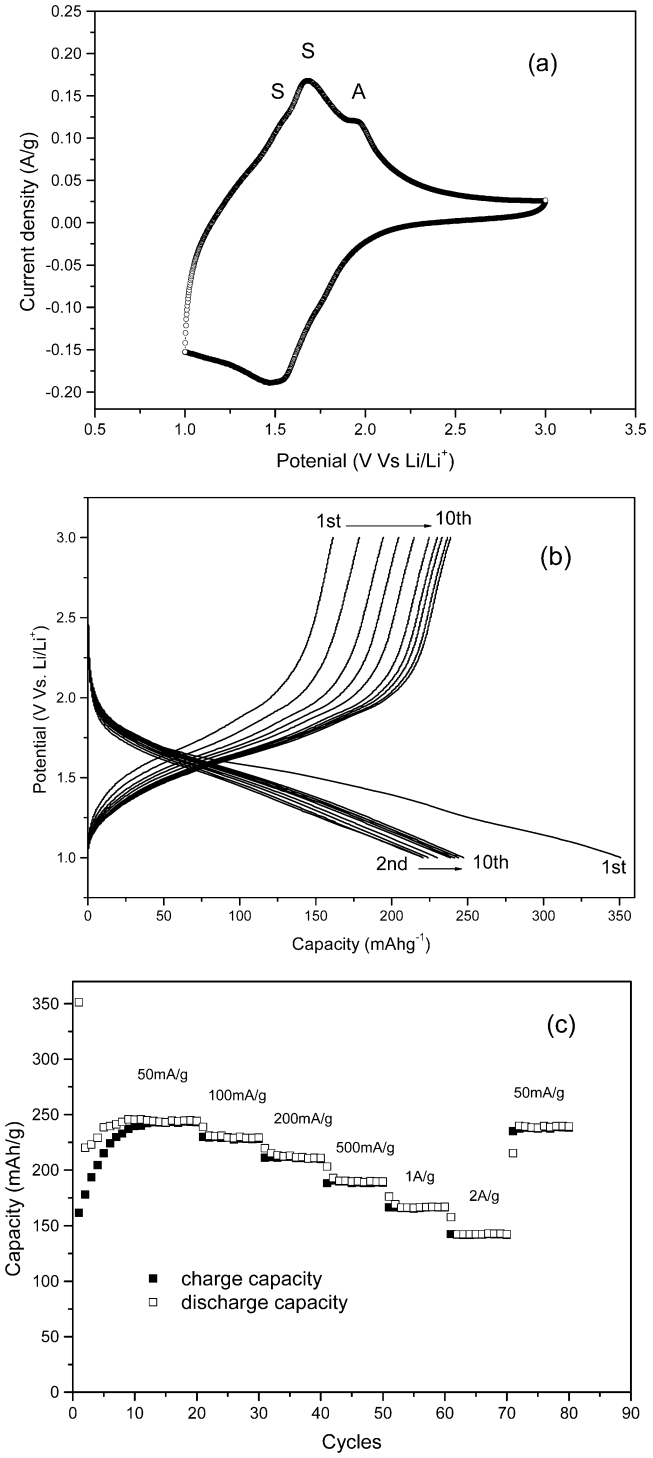

Figure 6. (a) cCyclic voltammograms of TiO_2(B)/anatase/carbon coating at the scan rate of 0.1 mV/s. (b) Galvanostatic discharge (lithium-insertion)/charge (lithium-extraction) curves vs. Li/Li^+ for TiO_2(B)/anatase/carbon coating at a current density of 50 mA/g. (c) Rate performance for TiO_2(B)/anatase/carbon coating.

coatings at a current density of 50 mA g^{-1} in the initial 10 discharge−charge cycles are shown. A high initial discharge capacity (350 mAh g^{-1}) was obtained, which reduced to 161 mAh g^{-1} in the following charge process, and thereafter slowly increased to 247 mAh g^{-1} after 10 cycles. A large capacity loss in the first cycle with nanostructured titania is common and may be due to surface reactions with the electrolyte on

dx.doi.org/10.1021/am4000744 | ACS Appl. Mater. Interfaces 2013, 5, 3631−3637

reduction. Unlike other reported TiO_2(B) nanomaterials, there is no obvious plateau at 1.70 or 1.50 V in the potential–capacity profiles; only a sloped discharge curve is observed, which agrees well with the aforementioned CV results.

The performance of the coatings is shown in Figure 6c at discharge current densities between 50 and 2000 mA g^{-1}. The cell was first cycled at 50 mA g^{-1}, where the specific capacity was 245 mAh g^{-1}. After 20 cycles at 50 mA g^{-1}, the current density increased gradually to 2000 mA g^{-1}. The reversible capacities were ~230, 212, 190, 167, and 143 mAh g^{-1} at current densities of 100, 200, 500, 1000, and 2000 mA g^{-1}, respectively. This performance is good among the reported data;[14−26] and more importantly, the unique electrode structure is free from binder additives and conductive agents, which are often used for powder samples. The high electrochemical performance is likely attributed to its unique electrode structure (3D porous conductive support and nanocarbon coating). These results open up the possibility to synthesize titania coatings for important device applications using a bioinspired route.

CONCLUSION

We have fabricated a protamine/titania composite layer on nickel foam through biomimetic layer-by-layer (LbL) titania mineralization. The coating was composed of amorphous carbon, TiO_2(B), and anatase titania nanoparticles, and the coating was formed upon organic pyrolysis under a reducing atmosphere. Most importantly, we formed the TiO_2(B) phase under mild conditions, which is usually prepared under harsh reaction conditions. Moreover, the obtained TiO_2(B)/anatase/carbon-coated nickel foam can be used as a binder-free electrode in lithium-ion batteries and exhibits high reversible capacity and fast charge–discharge properties. This suggests that such a benign and energy-efficient bioinspired route can be developed into a general pathway to synthesize titania coatings for various applications.

ASSOCIATED CONTENT

Supporting Information

Zeta potenial, Auger eelctron spectroscopy (AES), thermogravimetry (TG), X-ray diffraction (XRD), transmission electron microscopy (TEM), and X-ray photoelectron spectroscopy (XPS) measurement results. This information is available free of charge via the Internet at http://pubs.acs.org/

AUTHOR INFORMATION

Corresponding Author

* E-mail: chenge@bjut.edu.cn.

Present Address

[†]Department of Materials for Electronics, Institute of Materials Engineering and Institute of Micro- and Nanotechnologies MarcoNano, Ilmenau University of Technology, POB 100565, 98684 Ilmenau. Germany.

Author Contributions

The manuscript was written through contributions of all authors. All authors have given approval to the final version of the manuscript.

Notes

The authors declare no competing financial interest.

ACKNOWLEDGMENTS

This work was supported by the National Natural Science Foundation of China (NSFC No. 21001012) and Beijing Nova Program (No. 2009B06) and and the Scientific Research Common Program of Beijing Municipal Commission of Education (No. KM201210005005).

REFERENCES

(1) Mann, S. *Biomineralization: Principles and Concepts in Bioinorganic Materials Chemistry*; Oxford University Press: Oxford, U.K., 2001.
(2) Dickerson, M. B.; Sandhage, K. H.; Naik, R. R. *Chem. Rev.* **2008**, *108*, 4935–4978.
(3) Sumerel, J. L.; Yang, W.; Kisailus, D.; Weaver, J. C.; Choi, J. H.; Morse, D. E. *Chem. Mater.* **2003**, *15*, 4804–4809.
(4) Kisailus, D.; Choi, J. H.; Weaver, J. C.; Yang, W.; Morse, D. E. *Adv. Mater.* **2005**, *17*, 314–318.
(5) Smith, G. P.; Baustian, K. J.; Ackerson, C. J.; Feldheim, D. L. *J. Mater. Chem.* **2009**, *19*, 8299–8306.
(6) Chen, X. B.; Mao, S. S. *Chem. Rev.* **2007**, *107*, 2891–2959.
(7) Nonoyama, T.; Kinoshita, T.; Higuchi, M.; Nagata, K.; Tanaka, M.; Sato, K.; Kato, K. *J. Am. Chem. Soc.* **2012**, *134*, 8841–8847.
(8) Zhang, H.; Banfield, J. F. *J. Phys. Chem. B* **2000**, *104*, 3481–3487.
(9) Finnegan, M. P.; Zhang, H. Z.; Banfield, J. F. *J. Phys. Chem. B* **2007**, *111*, 1962–1968.
(10) Finnegan, M. P.; Zhang, H. Z.; Banfield, J. F. *Chem. Mater.* **2008**, *20*, 3443–3449.
(11) Kröger, N.; Dickerson, M. B.; Ahmad, G.; Cai, Y.; Haluska, M. S.; Sandhage, K. H.; Poulsen, N.; Sheppard, V. C. *Angew. Chem., Int. Ed.* **2006**, *45*, 7239–7243.
(12) Yang, Z. G.; Choi, D. W.; Kerisit, S.; Rosso, K. M.; Wang, D. H.; Zhang, J.; Graff, G.; Liu, J. *J. Power. Sources* **2009**, *192*, 588–598.
(13) Zukalova, M.; Kalbac, M.; Kavan, L.; Exnar, I.; Graetzel, M. *Chem. Mater.* **2005**, *17*, 1248–1255.
(14) Armstrong, A. R.; Armstrong, G.; Canales, J.; Bruce, P. G. *Angew. Chem., Int. Ed.* **2004**, *43*, 2286–2288.
(15) Armstrong, A. R.; Armstrong, G.; Canales, J.; Garcia, R.; Bruce, P. G. *Adv. Mater.* **2005**, *17*, 862–865.
(16) Bavykin, D. V.; Friedrich, J. M.; Walsh, F. C. *Adv. Mater.* **2006**, *18*, 2807–2824.
(17) Li, Q. J.; Zhang, J. W.; Liu, B. B.; Li, M.; Liu, R.; Li, X. L.; Ma, H. L.; Yu, S. D.; Wang, L.; Zou, Y. G.; Li, Z. P.; Zou, B.; Cui, T.; Zou, G. T. *Inorg. Chem.* **2008**, *47*, 9870–9873.
(18) Myung, S. T.; Takahashi, N.; Komaba, S.; Yoon, C. S.; Sun, Y. K.; Amine, K.; Yashiro, H. *Adv. Funct. Mater.* **2011**, *21*, 3231–3241.
(19) Li, J. M.; Wan, W.; Zhou, H. H.; Li, J. J.; Xu, D. S. *Chem. Commun.* **2011**, *47*, 3439–3441.
(20) Liu, H. S.; Bi, Z. H.; Sun, X. G.; Unocic, R. R.; Paranthaman, M. P.; Dai, S.; Brown, G. M. *Adv. Mater.* **2011**, *23*, 3450–3454.
(21) Beuvier, T.; Richard-Plouet, M.; Granvalet, M. M.; Brousse, T.; Crosnier, O.; Brohan, L. *Inorg. Chem.* **2010**, *49*, 8457–8464.
(22) Beuvier, T.; Richard-Plouet, M.; Brohan, L. *J. Phys. Chem. C* **2009**, *113*, 13703–13706.
(23) Liu, S. H.; Jia, H. P.; Han, L.; Wang, J. L.; Gao, P. F.; Xu, D. S.; Yang, J.; Che, S. A. *Adv. Mater.* **2011**, *24*, 3201–3204.
(24) Ren, Y.; Liu, Z.; Pourpoint, F.; Armstrong, A. R.; Grey, C. P.; Bruce, P. G. *Angew. Chem. Int. Ed.* **2012**, *51*, 2164–2167.
(25) Xiang, G.; Li, T.; Zhuang, J.; Wang, X. *Chem. Commun.* **2010**, *46*, 6801–6803.
(26) Kobayashi, M.; Petrykin, V. V.; Kakihana, M.; Tomita, K.; Yoshimura, M. *Chem. Mater.* **2007**, *19*, 5373–5376.
(27) Jiang, Y. J.; Yang, D.; Zhang, L.; Li, L.; Sun, Q. Y.; Zhang, Y. F.; Li, J.; Jiang, Z. Y. *Dalton Trans.* **2008**, 4165–4171.
(28) Fang, Y. N.; Wu, Q. Z.; Dickerson, M. B.; Cai, Y.; Shian, S.; Berrigan, J. D.; Poulsen, N.; Kroger, N.; Sandhage, K. H. *Chem. Mater.* **2009**, *21*, 5704–5710.
(29) Berrigan, J. D.; Kang, T. S.; Cai, Y.; Deneault, J. R.; Durstock, Sandhage, K. H. *Adv. Funct. Mater.* **2011**, *21*, 1693–1700.

(30) Haase, N. R.; Shian, S.; Sandhage, K. H.; Kroger, N. *Adv. Funct. Mater.* **2011**, *21*, 4243−4251.
(31) Jiang, Y. J.; Yang, D.; Zhang, L.; Sun, Q. Y.; Sun, X. H.; Li, J.; Jiang, Z. Y. *Adv. Funct. Mater.* **2009**, *19*, 150−156.
(32) Lee, H.; Dellatore, S. M.; Miller, W. M.; Messersmith, P. B. *Science* **2007**, *318*, 426−430.
(33) Yu, B.; Liu, J. X.; Liu, S. J.; Zhou, F. *Chem. Commun.* **2010**, *46*, 5900−5902.
(34) Xin, S.; Guo, Y. G.; Wan, L. J. *Acc. Chem. Res.* **2012**, *45*, 1759−1769.
(35) Wei, Q.; Zhang, F. L.; Li, J.; Li, B. J.; Zhao, C. S. *Polym. Chem.* **2010**, *1*, 1430−1433.
(36) Kavan, L.; Kalbac, M.; Zukalova, M.; Exnar, I.; Lorenzen, V.; Nesper, R.; Gratzel, M. *Chem. Mater.* **2004**, *16*, 477−485.
(37) Arrouvel, C.; Parker, S. C.; Islam, M. S. *Chem. Mater.* **2009**, *21*, 4778−4783.
(38) Armstrong, A. R.; Arrouvel, C.; Gentili, V.; Parker, S. C.; Islam, M. S.; Bruce, P. G. *Chem. Mater.* **2010**, *22*, 6426−6432.
(39) Dalton, A. S.; Belak, A. A.; Van der Ven, A. *Chem. Mater.* **2012**, *24*, 1568−1574.
(40) Wang, J.; Polleux, J.; Lim, J.; Dunn, B. *J. Phys. Chem. C* **2007**, *111*, 14925−14931.